 CMC, vol.51, no.1, pp.21-42, 2016

Research on the Damage of Porosityand Permeabilitydue to Perforation on Sandstone in the Compaction Zone

Shifeng Xue[1,2], Xiuxing Zhu[1,2], Lin Zhang[3], Shenghu Zhu[4], Guigen Ye[1], Xuejun Fan[5]

Abstract: A perforating hole is a channel through which the oil and gas in a reservoir pass into the production well bore. During the process of perforating due to explosion, the surrounding sandstone will be damaged to a certain extent, which will increase the well bore skin and lead to the decrease of production consequently. In this work a mechanical model of perforating damage is developed to describe the influences of perforating due to explosion on the porosity and permeability of the surrounding sandstone near the compaction zone. Based on this developed model, the important data related to the damage of sandstone, such as matrix effective stress, plastic deformation, volumetric strain, and so on, can be numerically simulated. Especially the behaviors of plasticity kinematic hardening at high strain rate due to impact loads, which are the important characteristics in the sandstone, is taken into account in this developed model. Both numerical and testing results show that the damage due to perforation in the sandstone can be accurately predicted by the developed model together with the porosity and permeability evolving model of perforation in a compaction zone. As a practical application, a methodology for the analysis of damage of porosity and permeability around a perforation tunnel is supposed based on the developed model and the core flow efficiency test of interparticle pore spaced sandstone target in China Shengli Oilfield and the computed tomography test.

1 Introduction

During the perforation process, the metal jet with high energy formed by the explosion of perforating charges penetrates the casing and sandstone formations, and

[1] Departmentof Engineering Mechanics, China University of Petroleum, Qingdao 266580, China
[2] Corresponding author: Prof. ShifengXue, sfeng@upc.edu.cn
Doc. Xiuxing Zhu, zhuxx99@upc.edu.cn
[3] Well Logging Company, ShengliOil Engineering Co., Ltd., Dongying 257000, China
[4] Schlumberger Drilling Dynamic Solution, Beijing 100022, China
[5] Department of Mechanical Engineering, Lamar University, Beaumont, TX 77710, USA

forms a channel of perforating hole that connects reservoirs to awell bore. The sandstone matrix and particles around a perforation channel are extruded by pressure loads due to the explosion, and constitute the complex crushed and compacted zone around the perforation channel, which damages the porosity and permeability of sandstone and leads to the sharp declining of the productivity of oil and gas wells [Swift (1998); Baumann and Brinsden (2014)]. It is important to explainthe mechanism of porosity and permeability damaging due to perforation in a compaction zone and develop a model to describe the porosity and permeability damaging for improving the production of oil-gas well [Nabipour, Sarmadivaleh, and Asadi (2010); Glenn, Serra, and Rodgers (2014); Heiland, Grove, and Harvey (2009)].

Untiltoday some work about the mechanism of sandstone damage under the load of low strain rate have been published and available [Bostrom, Chertov, and Pagels (2014); Veronika et al., (2010); Thurman et al., (1991); Sheldon (2006); Wong, David, and Zhu (1997)]. According to above work, the porosity reduction is caused by the plastic volume deformation of sandstone matrix. Based on this mechanism, Morris, Lomov, and Glenn (2001, 2003) established the porosity and permeability-evolving model of sandstone damaging zone.

The sandstone damage under the impact load of the perforation pressure at a high strain rate is mainly accorded to the standard of API RP 19B to broadly and qualitatively evaluate the extent of porosity and permeability damage [API RP 19B-2006 (2006); Hiltl, Hagelberg, and Swift (1999); Karacan and Halleck (2003); Halleck, karacan, and Hardesty (2004); Karacan, Grader, and Halleck (2001); Swift and Hagelberg (2000); Karacan and Halleck (2002)].

The structure and physical characteristics of sandstone particles in the compaction zone after perforation are evaluated based on the data of core flow efficiency (CFE) obtained by using the means of NMR, CT MPR and electron microscope, etc.. However, research is relatively scarce on the mechanics and on the quantitative model of macroscopic mechanical parameters that are related to the sandstone damage [James, Brooks, and Solutions (2011)].

In this paper, the preliminary mechanical model to evaluate the compaction damage of perforation in a sandstone reservoir is established based on the information available in literature, and presents a method of quantitative evaluation that combines the efficiency test of perforation with a numerical simulation [Karacan and Halleck (2003); Zhu, Zhang, and Xue (2014)] in order to further solve the problems of cost and time-effectiveness during the damage evaluation experiment of perforation. The method offers an effective way for the porosity and permeability damage evaluation of sandstone perforation.

The dynamic response of sandstone in the perforation compacting zone is simulated by nonlinear finite element method. The key data of matrix pressure, plastic deformation and volumetric strain, which are related to the sandstone damage of perforation compacting zone, can be obtained to quantitatively evaluate the extent of the porosity and permeability damage of a perforation compacting zone.

The applicability of the method proposed in this paper is proven by comparing the numerical simulation results of sandstone damage in a perforation compacting zone with the test data of CFE, CT MPR, and electron microscope analysis.

2 The model of porosity and permeability damage of the sandstone target

According to the dynamic response of sandstone under the impact load of perforation, the porosity and permeability-evolving model of sandstone under low strain rate is modified, and the preliminary mechanical model for evaluating the compaction damage of perforation in a sandstone reservoir is established.

Morris gives out the porosity and permeability-evolving model of sandstone under low strain rate, as seen in Formula (1)–(6) [Morris, Lomov, and Glenn (2003)]. The effective stress, plastic strain and damage variable of a sandstone unit are the parameters for the model calculation, which can be obtained by means of numerical analysis and will facilitate the analysis of porosity and permeability evolution.

$$\phi = \phi_d + \phi_c \tag{1}$$

$$\dot{\phi}_d = \frac{m_d \sigma_{vm} \dot{\varepsilon}_p (\phi_d^{\max} - \phi_d)}{\max(P_m, P_{\min})} \tag{2}$$

$$\phi_c^0 = \begin{cases} \Phi_I - P_{eff}(\Phi_I - (\Phi_* + CP*))/P* & for\ P_{eff} < P* \\ \Phi_* + CP_{eff} & otherwise \end{cases} \tag{3}$$

$$\phi_c = \frac{\phi_c^0}{1+A} \tag{4}$$

$$\dot{A} = c_1 \dot{\varepsilon}_p \min(P_{eff}, P_S^*) + c_2 H(P_{eff} - P*) \times H(P_{h2} - P_{eff}) \langle -\mathrm{trace}(D) \rangle \tag{5}$$

$$k = k_0 \exp\{K_I \phi_c(P_{eff}, A) - B \min(A, A^{\max})\} \tag{6}$$

Where $\phi_d^{\max}$ is the maximum swelled porosity; P_m is the average stress, with a unit of GPa; $P_{\min}$ is the minimum swelling stress, with a unit of GPa; ϕ_c^0 is the porosity of sandstone before damage; Φ_I is the initial porosity; Φ_* is the intercept of porosity; C is the rate of decay of porosity with a unit of GPa^{-1}; P_{eff} is the effective pressure, with a unit of GPa; A is the damage variable; c_1 is the loss factor of plastic strain; c_2 is the loss factor of hydrostatic pressure; P_S^* is the maximum damaging stress of plastic strain, with a unit of GPa; P_{h2} is the maximum damaging stress of hydrostatic pressure, with a unit of GPa; $H()$ is a step function; k is the

permeability coefficient, with a unit of mD; k_0 is the initial permeability, with a unit of mD; K_I is the relative index of permeability; B is the decay factor of permeability damage; $A_{\max}$ is the maximum damage variable.

In Morris' model, the parameter Φ_* is defined as the fluid porosity intercept, which refers to the porosity of sandstone when the effective stress reaches the critical hydrostatic pressure under a static loading. During the loading process of the impact load of perforation, the effective stress of sandstone will rapidly exceed the critical hydrostatic stress, thus the fluid porosity intercept Φ_* will change little comparing with the reference fluid porosity Φ_I, then it can be considered that $P_{eff} \geq P*$ and $\Phi_* = \Phi_I$, so Formula (3) can be modified as:

$$\phi_c^0 = \Phi_I + CP_{eff} \tag{7}$$

Based on the above analysis, the mechanical model to evaluate the damage of porosity and permeability in the compaction zone of sandstone perforation can be established as equation (8)–(10).

$$\phi = \Phi_I - \exp\left\{\frac{m_d \sigma_{vm}(\varepsilon_{p1} - \varepsilon_{p2})}{\max(P_m, P_{\min})} t\right\} + \frac{\Phi_I + CP_{eff}}{1 + A} \tag{8}$$

$$k = k_0 \exp\left\{\frac{K_I(\Phi_I + CP_{eff})}{1 + A}(P_{eff}, A) - B\min(A, A^{\max})\right\} \tag{9}$$

Where the damage variable A can be derived according to Formula (5) as:

$$A = c_1 \varepsilon_p \min(P_{eff}, P_S^*) + c_2 H(P_{eff} - P^*) \times H(P_{h2} - P_{eff}) \max(0, \varepsilon_v) \tag{10}$$

Where ε_p is the plastic strain of sandstone unit andε_v is the volumetric strain of the sandstone unit. c_1 is the loss factor of plastic strain with unit of GPa^{-1} and c_2 is the damage factor of hydrostatic pressure. Furthermore, p_s^* is the maximum damaging stress of plastic strain with unit of GPa, p^* is the critical pressure of hydrostatic pressing compaction with unit of GPa, and P_{h2} is the maximum damaging stress of hydrostatic pressing compaction with unit of GPa. $H()$ is a step function. The values of the parameters are shown in Table 1.

This study defined the evaluation indexes ϕ_{cd} and k_{cd} of porosity & permeability damage extent as:

$$\phi_{cd} = \frac{\Phi_I - \bar{\phi}}{\Phi_I} \times 100\% \tag{11}$$

$$k_{cd} = \frac{k_0 - \bar{k}}{k_0} \times 100\% \tag{12}$$

Where ϕ_{cd} is the damaged extent of porosity. k_{cd} is the damage extent of permeability. $\bar{\phi}$ is the average porosity of compaction zone. $\bar{k}$ is the average permeability of compaction zone, with the unit of mD.

3 Quantitative analysis of the macro-mechanical parameter of sandstone in compaction zone

During the perforation process, sandstone is subjected to the impact load that generates plastic shear, squeezing and complex deformations associated with interparticle dislocation. This paper applied the deformation characteristic of sandstone from the characterized high strain rate of plasticity in a kinematic hardening material model under impact loads [Yang (2012)]. The numerical simulation of the dynamic response of sandstone in the compaction zone of perforation was performed, which provided the key macroscopic mechanical parameters of sandstone matrix pressure, plastic deformation and volumetric strain. It also provided the essential data for the quantitative evaluation of the porosity and permeability damage in a compaction zone.

3.1 Essential data

Based on the performance test of sandstone target core, properties needed for perforating damage in the compaction zone were obtained as shown in Table 1.

3.2 Numerical model

Considering that the structure of a sandstone target is axially symmetric, the numerical model of sandstone under the impact load of perforation was established as shown in Figure 1.

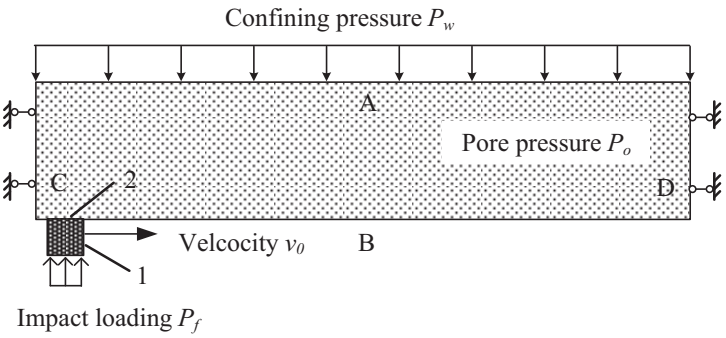

Figure 1: The numerical model of sandstone under the impact load of perforation.

In order to simulate the actions of shear, friction and squeezing on the sandstone of the inner wall in the perforating hole by the impact load during the perforating process of a perforating metal jet, this study assumed a rigid unit block in the model, which experienced an axial motion along the perforating hole. The pressure pulse load was forced on the Boundary 1. Boundary 2 came in contact with the boundary

Table 1: Essential Properties of Sandstone.

Symbol	Meaning	Value
C	Decay rate of porosity	-0.11 GPa^{-1}
c_1	Loss factor of plastic strain	29 GPa^{-1}
c_2	Loss factor of hydrostatic pressure	28.5
C_q	Material constant controlling plastic strain rate	0.31
m_d	Material constant controlling swelled porosity	124
$P_{\min}$	Minimum swelling stress	0.02 Gpa
$\phi_{dil}^{\max}$	Maximum swelled porosity	0.13
p_s^*	Maximum damaging stress of plastic strain	0.23 Gpa
p^*	Critical pressure value of hydrostatic pressure	4.8 GPa
P_1	constant representing plastic strength of material	1.54
$_{Ph2}$	Maximum damaging stress of hydrostatic pressure	0.42 Gpa
$A^{\max}$	Maximum damage variable	0.14
K_I	Relative index of permeability	54.6
B	Decay factor of permeability damage	12
Φ_I	Initial porosity	0.108
k_0	Initial permeability	3.4 mD
σ_y	Static yield stress	0.094 GPa
ρ	Density	2630 kg/m^3
E	Elasticity modulus	17 GPa
E_p	Plastic intensity modulus	0.93 GPa
ε_{eff}^p	Equivalent plastic strain	0.11
μ	Poisson's ratio	0.33
K_1	Horizontal permeability	2.6 mD
K_2	Vertical permeability	3.4 mD

CD of the inner wall in the perforating hole. The velocity v_0 of the rigid unit block was set same as the forming speed of the perforating hole.

3.3 Dynamic response analysis of sandstone close to a perforating hole

3.3.1 Pressure impact load

After the charge perforation is detonated, the resulting particle flow of metal with high speed will penetrate the casing, impact sandstone and form a huge impact load. Then,the load will induce a huge lateral pressure in the sandstone, squeeze the particles of sandstone and form a perforating hole.

So far, the lateral pressure pulsing load in the inner wall and the forming speed of a perforating hole cannot be obtained through experiments. They can only be

estimated by the method of numerical simulation. Literature suggests that for the conventional perforating charge, the peak value of pressure pulse load in the inlet end of a perforating hole is 10 GPa [Baumann and Brinsden (2004)]. The peak value at the bottom is declined to 1/10 of that in the inlet end of the perforating hole. The forming speed of the perforating hole is about 2000 m/s.

Assuming that the pressure impact load is linearly decreased, the peak load along the axis of perforating hole can be obtained as:

$$P_f = -\frac{9}{D}L_d + 10 \tag{13}$$

Where: P_f is the peak value, with unit of GPa. L_d is the length from the inlet end of the perforating hole, with unit of m. D is the depth of the perforating hole, which was selected as 0.56 m in this study.

3.3.2 Algorithm of contact-impact interface

Contact-impact interface involves complex nonlinear deformation. To solve such a complex issue, the selection of interfacial algorithm is very important [Rubin, Vorobiev, and Glenn (2000); Rbewi and Tiab (2012)].

In this paper, the penalty function method was adopted to process the contact-impact interface. The ultimate principle can be described as follows.

In every time step, the first step is to check whether the principal plane is penetrated from each slave node. No treatment is needed if there is no penetration. If there is a penetration, a contact force will exist at the interface between the slave node and the penetrated principal plane. The force is proportional to the depth of penetration and the rigidity of the principal plane, and is represented by a function named as the penalty function. That is:

$$f_s = -l_c k_i n_i \tag{14}$$

Where f_s is the contact force vector at the contact node and normal to the contact plane, l_c is the depth of penetration, with unit of mm. n_i is the outer normal unit vector of the master slice S_i at the point of contact. k_i is the stiffness factor of the master slice S_i.

3.3.3 Material model

Under the impact load of perforation, the strain rate of sandstone increases. Meanwhile, the relationship of stress-strain tends to be complex. Some essential parameters, such as yield limit and instant aneousstress, change in varying degrees. All of them influence on the dynamics response of sandstone. In order to represent

the mechanical property of sandstone under the condition of high strain rate, the plastic-kinematics hardening nonlinear material model, which contains the strain rate effect, was adopted. The following expression represents the relationship between the dynamic-limit yield stress and the strain rate of material in the model:

$$\sigma_d = \left[1 + \left(\frac{\dot{\varepsilon}}{C_q}\right)^{1/p_1}\right](\sigma_y + \beta E_p \varepsilon_{eff}^p) \tag{15}$$

Where σ_d is the dynamic-limit yield stress, with unit of MPa, $\dot{\varepsilon}$ is the strain rate, with unit of s^{-1}, and C_q and P_1 are the constants which are related to the material property. σ_y is the static yield stress with unit of MPa. β is the hardening parameter, which is zero for the plastic-kinematics hardening model. E_p is the plastic-kinematics hardening modulus, with unit of GPa. ε_{eff}^p is the equivalent plastic strain.For the inter-particle pore of sandstone,the values of relevant parameters can be seen in Table 1.

3.3.4 Mesh generation

Two-dimensional physical unit with four nodes of PLANE 162 was used to map the mesh of the model. The mesh density was determined according to the accuracy requirement.

A trial mesh generation suggested that the length AB in the model (Figure 1) be divided into 900 segments and the width AC be divided into 90 segments. Then, each unit could be expressed by serial number r_{ij} $(i = 1,2,\ldots m; j = 1,2,\ldots,n)$ where $m = 900$ and $n = 90$. The resulting data for a unit can be expressed by an array R, as seen in Formula (16).

$$R = \begin{bmatrix} r_{11} & r_{12} & \ldots & r_{1n} \\ \vdots & \vdots & r_{ij} & \vdots \\ r_{m1} & r_{m2} & \ldots & r_{m,n} \end{bmatrix} \tag{16}$$

3.3.5 The macroscopic mechanical parameter analysis of sandstone in the compaction zone

Dynamic response of sandstone in the compacting zone during the process of perforation was simulated numerically. The radial displacement of sandstone in the process of perforating and compacting was obtained as illustrated in Figure 2.

Mechanical parameters, such as displacement, stress and plastic strain, were extracted from each node, and were assigned to the corresponding arrays of R_{ux}, R_{uy}, $R_{\sigma x}$, $R_{\sigma y}$, $R_{\varepsilon px}$ and $R_{\varepsilon py}$. According to formulas (17) and (18), the effective stress and volumetric strain of a sandstone unit can be computed as:

$$P_{eff} = (\sigma_x + \sigma_y)/2 - P_0 \tag{17}$$

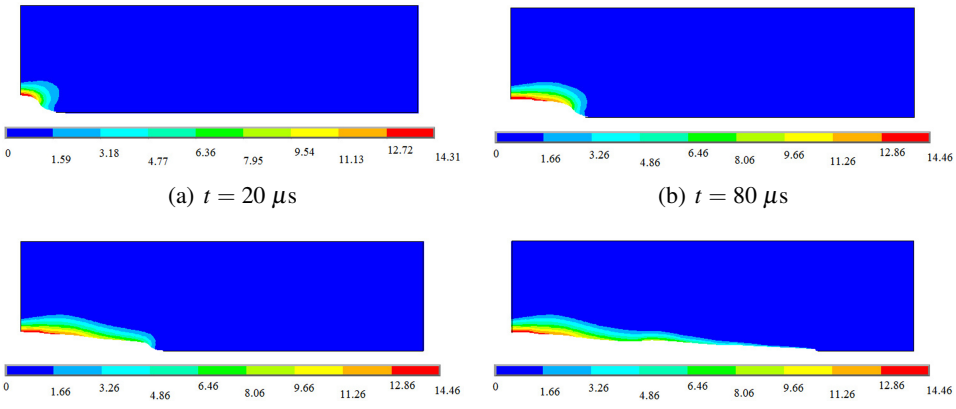

(a) $t = 20\ \mu$s (b) $t = 80\ \mu$s

(c) $t = 160\ \mu$s (d) $t = 280\ \mu$s

Figure 2: The radial deformation of sandstone in the process of perforating and compacting (mm).

$$\varepsilon_v = \varepsilon_x + \varepsilon_y \tag{18}$$

where σ_x is the x directional stress with a unit of GPa, σ_y is the y directional stress with a unit of GPa, P_0 is the pore pressure with unit of GPa, and ε_v is the volumetric strain of the sandstone unit. ε_x and ε_y are,respectively, the x and y directional strains of the unit.

The damage variable A of the sandstone unit can be solved according to Formula (10), then, according to Formula (8) and (9), the distribution of porosity and permeability of sandstone can be obtained.

4 Test on sandstone target in a perforation compaction zone

By using a CFE detection device with ultra-temperature and high pressure from the logging company of Shengli Oil Field as a platform, and following the standard procedure of API RP 19B, this study simulated the perforating process of sandstone target between inter-particle pores under the environments of reservoir and well-bore (bottom hole temperature, pressure of well-bore, pore pressure, and pressure of overlying strata [API RP 19B-2006 (2006)].

Meanwhile, the sandstone target and the perforating gun and charges were designed according to the experimental flow recommended in the API RP 19B Standard as [API RP 19B-2006 (2006)].

The outer diameter of sandstone target was 160 mm with the length of 800 mm; the porosity was 10.8% and the permeability was 3.4 mD.

The charge type was DP44RDX32-5, with the explosive of RDX and the charge

amount of 32 g.

During the whole perforating process, the parameters were kept as below: the temperature of sandstone target was 80°C. The pressure of well bore was 10 MPa. The confining pressure was 35 MPa, and the pore pressure was 20 MPa.

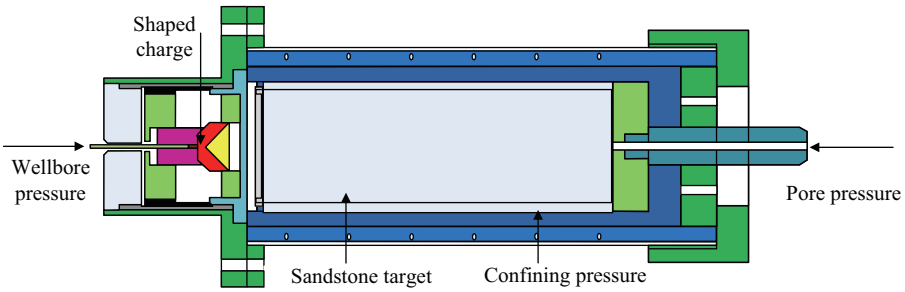

Figure 3: Core holder and simulated well bore assembly.

Table 2: CFE Test Data of Sandstone Target.

Time (s)	Confining Pressure (MPa)	Pore Pressure (MPa)	Effective Stress (MPa)	Pressure Difference (MPa)	Flow (ml)
1200	35.1	20	15.1	20	3.5
1200	35.3	20	15.3	20	3.3
1200	35.2	20	15.2	20	3.6
1200	35.2	20	15.2	20	3.2
1200	35.4	20	15.4	20	3.4
Average			3.4		

4.1 CFE test of sandstone target

During the experiment, by maintaining the confining pressure and pore pressure constant after perforation, the fluid flow (kerosene) in the sandstone target perforated channel under the constant pressure difference was obtained, which can be seen in Table 2.

The CFE of perforation can be calculated from Formula (19) as API RP 19B-2006 (2006)

$$CFE = \frac{1.25 - \ln(r)}{1.25 - \ln(r) + \ln(\frac{R}{r})(\frac{Q_c}{Q_m} - 1)} \tag{19}$$

Where r is the perforating radius with unit of m, R is the core radius with unit of m, Q_c is the theoretical calculation flow with unit of m^3/s, and Q_m is the measured flow with unit of m^3/s.

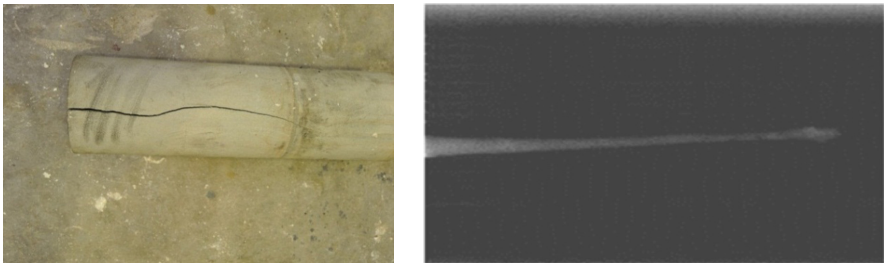

(a) (b)

Figure 4: The shape of a sandstone target perforating hole.

Q_c can be calculated as

$$Q_c = 1.08 \times 10^{-3} \frac{\Delta P}{\mu} \left[\frac{K_1 D}{\ln(\frac{R}{r})} + \frac{K_2 r R}{R - r} \right] \tag{20}$$

Where ΔP is the pressure difference between confining pressure and effective stress of sandstone target, with unit of Pa, μ is the viscosity of kerosene with unit of $Pa \cdot s$, D is the perforating depth with unit of m. While K_1 is the horizontal (axial direction of perforating hole) permeability, with unit of m^2, K_2 is the vertical permeability, with unit of $m^2 \cdot K_1$ and K_2 can be obtained by testing the core sample of sandstone target with a Hassler Permeameter.

4.2 CT scan of perforating sandstone target

Figure 4 shows the shape of a sandstone target perforating hole after perforation. By analysis, the perforating depth D was 560 mm, with the average perforating radius r of 12.2 mm.

This study selected the cross sections of six sandstone targets, which are located with different lengths (L_d) from the entrance of the perforating hole, as shown as Figure 5. CT scan was performed for the sandstone target after drying and for the sandstone target saturated with water to obtain the CT distributions in the different cross sections. The porosity distributions of sandstone targets in different cross sections are obtained according to Formula (21) as Karacan and Halleck (2003)

$$\phi = \frac{\lambda_{rw} - \lambda_{ra}}{\lambda_w - \lambda_a} \tag{21}$$

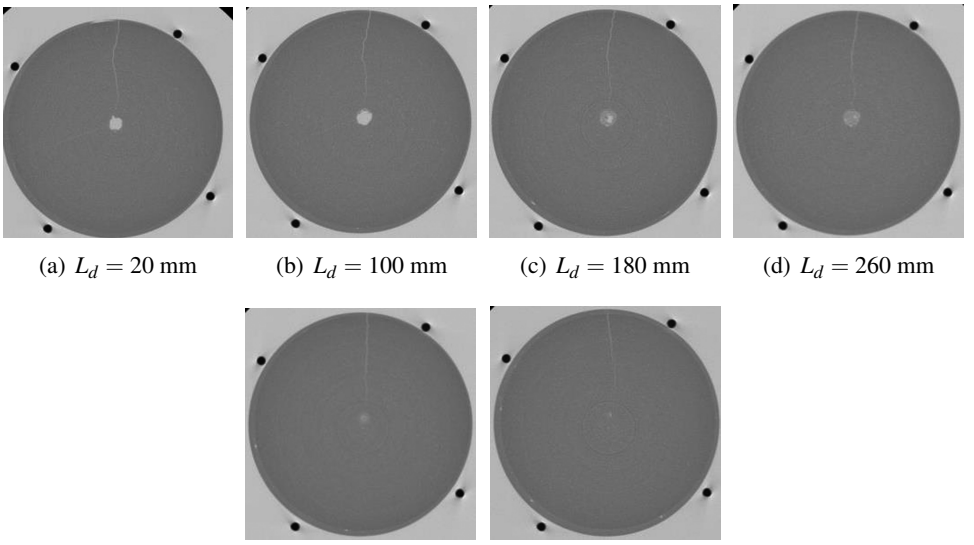

(a) $L_d = 20$ mm (b) $L_d = 100$ mm (c) $L_d = 180$ mm (d) $L_d = 260$ mm

(e) $L_d = 320$ mm (f) $L_d = 500$ mm

Figure 5: The radial CT scanning imageries of sandstone targets in different locations.

Where λ_{rw} is the CT number of sandstone targets with saturated water in the cross sections, λ_{ra} is the CT number of sandstone targets after drying in the cross sections, λ_w is the CT number of water, and λ_a is the CT number of air. The CT number of saturated water that was selected in the experiment was $\lambda_w = 52$ H. While, the CT number of air was $\lambda_a = -1000$ H.

CT scanning data of the sandstone target cross-sections were statistically analyzed to obtain the distribution of porosity on the cross sections as shown in Figure 6 [Karacan and Halleck (2003); Karacan, Grader, and Halleck (2001)]. Based on this porosity distribution, the permeability distribution on the cross-sections was determined according to the calculation method as proposed by Karacan, Grader, and Halleck (2001), the permeability distribution is shown in Figure 7 [Karacan, Grader, and Halleck (2001)].

5 Evaluation of the porosity and permeability damage of the sandstone target

5.1 Distribution of porosity

Figure 8 (a) and Figure 8 (b) present the experimental data and numerical analysis results of the radial porosity distribution for the sandstone target cross sections

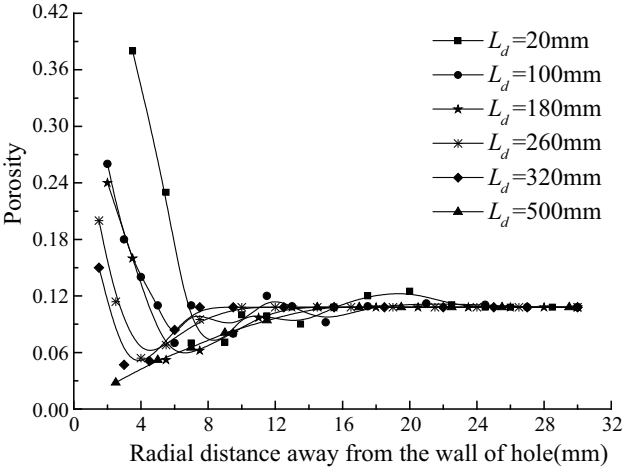

Figure 6: The radial porosity distribution of sandstone target.

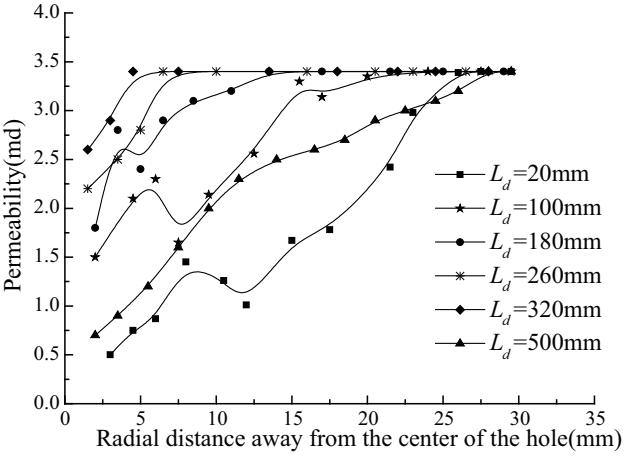

Figure 7: The radial permeability distribution of sandstone target.

located at distances of $L_d = 20$ mm and $L_d = 100$ mm to the inlet end of the perforating hole. The results of numerical calculation well agree with the results of experiments.

Due to the strong shear action on the inner wall of perforation hole by the impact load, the shear swelling for sandstone was formed on the surface layer of the inner wall in the perforation hole, thus, increasing the porosity of sandstone (corresponding to the experimental observation that sandstone in the internal surface of a perforation hole was fractured forming fine map cracks as shown in Figure 9. In

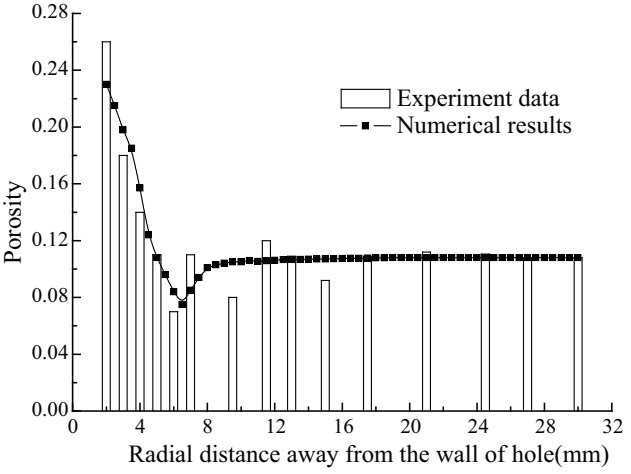

(a) The radial porosity distribution in the cross section at $L_d = 20$ mm

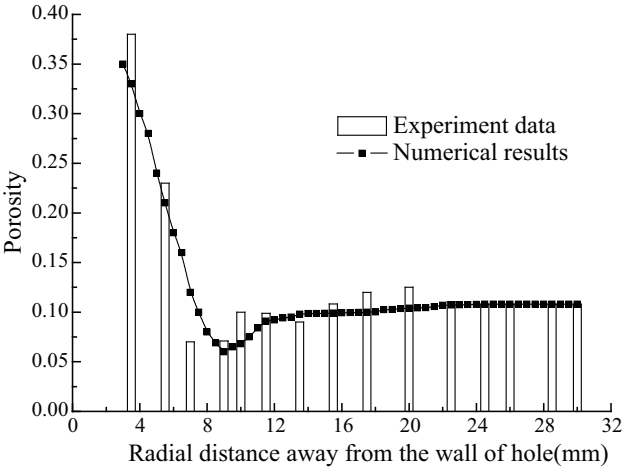

(b) The radial porosity distribution in the cross section at $L_d =$ 100 mm

Figure 8: The porosity distribution of sandstone perforation in the compaction zone.

about 3 mm from the inner wall of perforation hole, the porosity of sandstone was greater than the initial porosity.

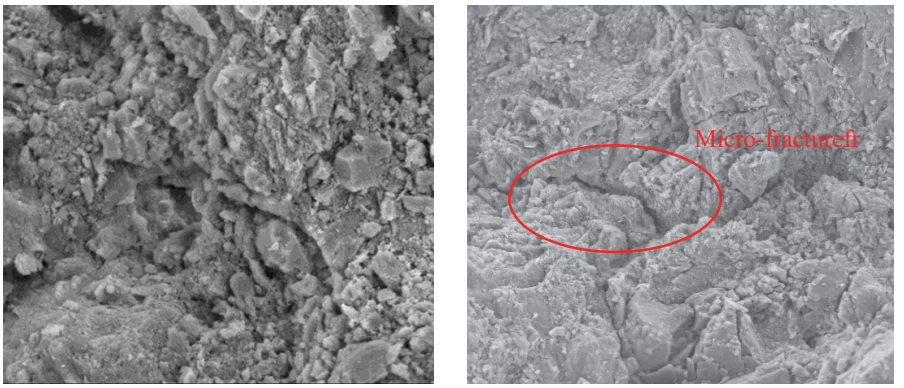

(a) (b)

Figure 9: Scanning electron microscope images. (a) Uncompacted status; (b) Micro-fracture of the inner wall in the perforation hole.

5.2 Distribution of permeability

Figure 10 shows the radial permeability distribution of sandstone corresponding to $L_d = 20$ mm and $L_d = 100$ mm. It is known from the experimental data and the results from the numerical analysis that the severest damage of permeability occurred on the surface of the inner wall in the perforation hole. The extent of damage declined with an increase in radial distance.

Since the map cracks were not only narrow, but also offered a greater resistance and a poorer flow ability than that by the initial pore structure, the superficial sandstone permeability of the inner wall in the perforation hole didnot follow the change law same as that by porosity.

During the experiment, the negative pressure of well bore after the completion of perforation lowered down the damage extent and improved the permeability and flow capacity for cleaning the chippings of perforation hole. This point was not considered in the numerical model. Therefore, the sandstone permeability near the perforation hole was lower in the results of numerical analysis.

5.3 Evaluation of the Extent of Damage

Based on the CFE tested data of sandstone target perforation (see Table 2), CFE = 60.1% can be obtained from Formula (19) and Formula (20). Where r is 6.1 mm, R is 80 mm, ΔP is 20 MPa, μ is 1.7 MPa.s, and D is 560 mm. K_1 is 2.6 mD $\cdot$ K_2 is 3.4mD $\cdot$ Q_c is 0.00747 ml/s and Q_m is 0.00283 ml/s.

The extent of damage can be evaluated by combining the results of the numeri-

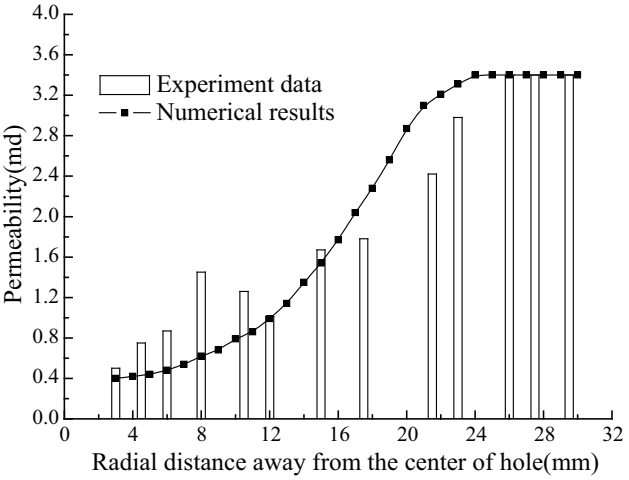

(a) The radial permeability distribution in the cross section of $L_d = 20$ mm

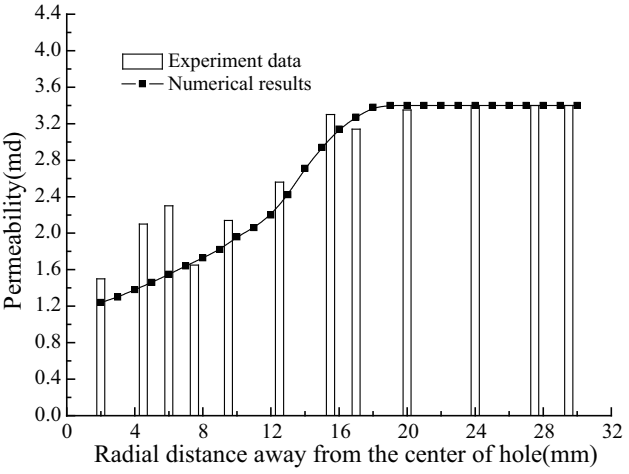

(b) The radial permeability distribution in the cross section of $L_d = 100$ mm

Figure 10: The radial permeability distribution of sandstone.

cal analysis and by means of quantitatively describing the porosity distribution of sandstone.

Twenty measuring points were selected along perforaction hole distance. Radial porosity and permeability data of sandstone were extracted from the corresponding positions, and solved for their average value. According to Formulas (11) and (12),

Table 3: The damage extent evaluation of perforating porosity and permeability in the compaction zone.

Length to Inlet End (mm)	Thickness of Compaction Zone (mm)	Average Porosity	Damage extent of Porosity (%)	Average permeability (md)	Damage extent of Permeability (%)
10	20.4	0.052	51.85	0.45	86.76
40	16.7	0.056	48.15	0.49	85.59
70	13.2	0.061	43.52	0.52	84.71
100	11.8	0.069	36.11	0.59	82.65
130	8.6	0.074	31.48	0.67	80.29
160	7.3	0.079	26.85	0.71	79.12
190	6.5	0.082	24.07	0.76	77.65
220	5.8	0.095	12.04	0.85	75.00
250	5.2	0.097	10.19	1.01	70.29
280	4.9	0.101	6.48	1.15	66.18
310	4.6	0.102	5.56	1.48	56.47
340	4.1	0.102	5.56	1.65	51.47
370	3.4	0.103	4.63	1.9	44.12
400	2.9	0.103	4.63	2.16	36.47
430	2.6	0.104	3.70	2.38	30.00
460	2.3	0.106	1.85	2.74	19.41
490	1.8	0.107	0.93	3.01	11.47
520	1.2	0.108	0.00	3.25	4.41
550	0.8	0.108	0.00	3.4	0.00
Average Value	6.5	0.089	16.7	1.53	54.85

the extent of damage due to perforation in a compaction zone was quantitatively evaluated. The numerical results are shown in Table 3. The curve of thickness of compaction versus perforaction hole distance, the curves of average porosity versus perforaction hole distance, and the curves of average permeability versus perforaction hole distance are ploted in Figures 11, 12, and 13, respectively.

Table 3 shows that the average compacted thickness of perforation hole is 6.5 mm. The average porosity in the compacted zone is 0.089, and the damage extent is 16.7%. While, the average permeability in the compacted zone is 1.53 mD, the damage extent is 54.85%. According to figures 11, 12 and 13, the sandstone matrix was subjected to the squeezing action of the impact load in a 400 mm range along the axis of the sandstone-perforating hole, which generated the compacted zone with a thickness of 7 mm.

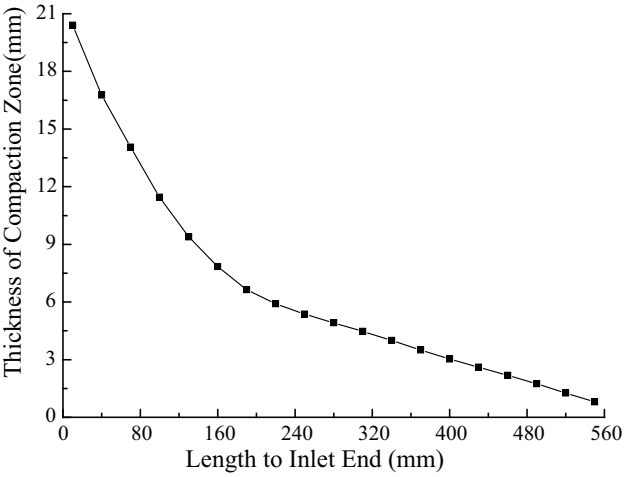

Figure 11: Curve of thickness of compaction versus perforaction hole distance.

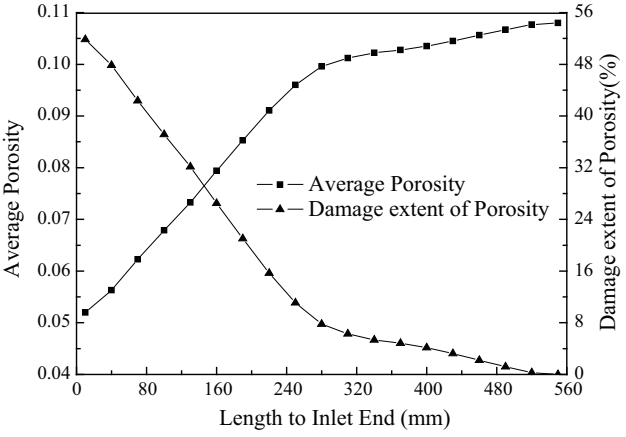

Figure 12: Curves of average porosity versus perforaction hole distance.

The deceased percentages of porosity and permeability are calculated based on the results of numerical caltionlation in Table 3. The deceased values of porosity and permeability are 16.7% and 54.85%, respectively.

Comparison with the test results of CFE provided that the error of numerical analysis for permeability damage extent was 8.7%, which further verified the reliability of the quantitative method.

According to this method, the porosity and permeability damage extents of perforation in the compacted zone under different operating conditions can be evaluated. Meanwhile, the corresponding map can be drawn. All of these can serve as a ref-

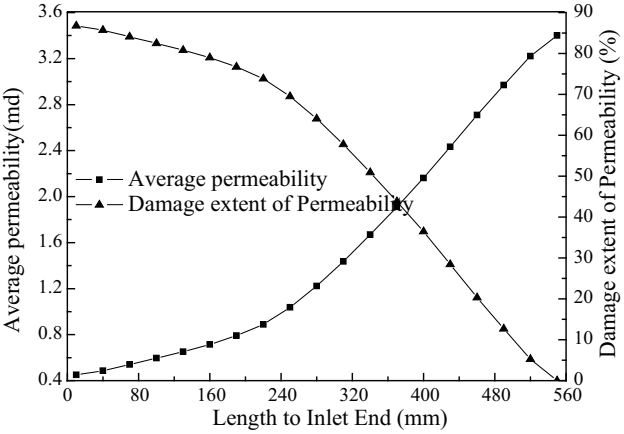

Figure 13: Curves of average permeability versus perforaction hole distance.

erence to match the perforating charge with the stratum and to optimize the design parameters of perforation.

6 Conclusion

(1) A plastic-kinematics hardening nonlinear model which contained the strain rate effect was proposed to describe the mechanical behaviors of sandstone upon impact loads with high strain rate of perforation.The dynamic response of the sandstone in the compacted zone of perforation was quantitatively evaluated by numerical simulation. This work provided an important numerical simulation method for the quantitative evaluation of damage in the compacted zone. The numerical results well agreed with the experimental results, which verified the effectiveness of the method.

(2) The supposed numerical simulation model can be used to efficiently evaluate the porosity and permeability damage extents of perforation in the compacted zone under different operating conditions together with the experimental data. Therefore it can serve as a reference to match the perforating charge with the stratum and to optimize the design parameters of perforation.

(3) The results of numerical analysis show that two important mechanisms related to the damage of sandstone in the compacted zone caused by the high-pressure metal jet are plastic squeezing and shear swelling.The damage extents of sandstone thickness in the compacted zone, porosity and permeability declined with the decline of pressure and load along the axial direction of the perforation hole.

(4) During the process of charge perforation, the actions of shear, friction and squeezing by the impact load caused the slippage/breaking of sandstone particles and the compaction/ fragmentation of matrix [Rubin, Vorobiev, and Glenn (2000); Rbewi and Tiab (2012)]. The damage mechanism of sandstone reservoir by perforation is very complex, which needs to be further researched in future.

Acknowledgement: This work was supported by the National Key Technologies Major Program of China (2011ZX05006-002).

Thanks to engineers Yungang Liu and Maiquan Zhang from the Super-high Temperature & High Pressure CFE Lab of SLOF Logging Company for the help in the aspects of core essential data and CFE test of perforating target.

Also, thanks to Dr. Han Zhidong of Liver more Software Technology Corp, USA, and Dr. Jie Wu of San Ying Precision Engineering Research Center for providing the technical supports in the aspects of Dyna numerical simulation and CT analysis of sandstone.

References

API RP 19B-2006. (2006): Recommended practices for evaluation of well perforators. *Washington, API Publishing Services*.

Baumann, C. E.; Brinsden, M. S. (2014): Perforating Gunshock Loads: Simulation and Optimization in 2014, SPE-170552-MS.

Bostrom, N.; Chertov, M.; Pagels, M. (2014): The Time-Dependent Permeability Damage Caused by Fracture Fluid, SPE-168140-MS.

Glenn, T. S.; Serra, M.; Rodgers, J. P. (2014): Investigating the Dynamic 3D Loading Effects on Perforating Guns Imposed by Shaped Charges-Downhole Evaluation, OTC-24891-MS.

Halleck, P. M.; karacan, C. O.; Hardesty, J. (2004): Changes in perforation-induced formation damage with degree of underbalance: comparison of sandstone and limestone formations. *SPE* 86541.

Heiland, J. C.; Grove, B. M.; Harvey, J. P. (2009): New fundamental insights into perforation-induced formation damage, SPE-122845-MS.

Hiltl, M.; Hagelberg, C. R.; Swift, R. P. (1999): Dynamic response of Berea sandstone shock-loaded under dry, wet and water-Pressurized conditions. *International Conference on High Pressure Science and Technology Honolulu*, National Technical Information Service, July 25–30, pp. 72–77.

James, E.; Brooks, P. R. J.; Solutions, D. H.; etc. (2011): Laboratory simulation of flow through a perforation, *SPE* 144187.

Karacan, C. O.; Grader, A. S.; Halleck, P. M. (2001): Mapping of permeability damage around perforation tunnels. *Journal of Energy Resources Technology*, vol. 123, no. 2, pp. 125–136.

Karacan, C. O.; Halleck, P. M. (2002): Correlating Particle Size Distribution in a Crushed Zone to Perforating Permeability Damage and Modeling Using Fragmentation Fractal Theory, SPE-77365-MS.

Karacan, C. O.; Halleck, P. M. (2003): Comparison of shaped-charge perforating induced formation damage to gas and liquid-saturated sandstone samples. *Journal of Petroleum Science and Engineering*, vol. 40, no. 3, pp. 61–75.

Morris, J. P.; Lomov, I. N.; Glenn, L. A. (2001): Simulating perforation permeability damage and cleanup. *Society of Petroleum Engineers*, vol. 23, no. 4, pp. 120–137.

Morris, J. P.; Lomov, I. N.; Glenn, L. A. (2003): A constitutive model for stress-induced permeability and porosity evolution of Berea sandstone. *Journal of Geophysical Research*, vol. 108, no. B10, pp. 2485–2496.

Nabipour, A.; Sarmadivaleh, M.; AsadiM, S. (2010): A DEM Study On Perforation Induced Damaged Zones And Penetration Length In Sandstone Reservoirs, ARMA-10-248.

Rbewi, S. A.; Tiab, D. (2012): Locating closed perforation zones and damaged section using well test analysis, *SPE* 161000.

Rubin, B.; Vorobiev, O. Y.; Glenn, L. A. (2000): Mechanical and numerical modeling of a porous elastic-viscoplastic material with tensile failure. *International Journal of Solids and Structures*, vol. 37, no. 7, pp. 1841–1871.

Scott, T. E.; Nielsen, K. C. (1991): The effects of porosity on the brittle-ductile transition in sandstones. *Journal of Geophysical Research*, vol. 96, no. B1, pp. 405–414.

Sheldon, H. A. (2006): Numerical modelling of faulting and fluid flow in porous rocks: An approach based on critical state soil mechanics. *Journal of Structural Geology*, vol. 28, pp. 1468–1482.

Swift, R. P. (1998): Micro-mechanical modeling of perforating shock damage. *SPE* 39458.

Swift, R. P.; Hagelberg, C. T. (2000): Modeling stress-induced damage from impact recovery experiments, *Proceedings of the ETCE/OMAE 2000 Joint Confer-*

ence on Energy for the New Millennium, ASME Conference Publishing Services, February, vol. 14–17, pp. 50–59.

Vajdova, V.; Zhu, W.; Chen, T. N. (2010): Micromechanics of brittle faulting and cataclastic flow in tavel limestone. *Journal of Structural Geology*, vol. 32, no. 1, pp. 1158–1169.

Wong, T. F.; David, C.; Zhu, W. (1997): The transition from brittle faulting to cataclastic flow in porous sandstones: Mechanical deformation. *Journal of Geophysical Research*, vol. 102, no. B2, pp. 3009–3024.

Yang, G. (2012): Plastodynamics (3rd Edition, in Chinese), China Higher Education Press.

Zhu, X.; Zhang, L.; Xue, S. (2014): Evaluation of perforating damage for sandstone. *Journal of China University of Petroleum (in Chinese)*, vol. 38, no. 1, pp. 37–42.